Open Access on 08/28/2015

ARTICLE

Sensitive and Selective Plasmon Ruler Nanosensors for Monitoring the Apoptotic Drug Response in Leukemia

Cheryl A. Tajon,[†,#] Daeha Seo,[‡,§,⊥] Jennifer Asmussen,[∥] Neil Shah,[∥] Young-wook Jun,[‡,*] and Charles S. Craik[†,*]

[†]Department of Pharmaceutical Chemistry, University of California, San Francisco, California 94158, United States, [‡]Department of Otolaryngology, University of California, San Francisco, California 94115, United States, [§]Department of Chemistry, University of California, Berkeley, California 94720, United States, [⊥]Materials Science Division, Lawrence Berkeley National Laboratory, Berkeley, California 94720, United States, and [∥]Department of Pharmaceutical Sciences and Pharmacogenomics, University of California, San Francisco, California 94143, United States. [#]Present address: The Molecular Foundry, Lawrence Berkeley National Laboratory, 1 Cyclotron Road, Bldg 67, Berkeley, CA 94720, U.S.A.

ABSTRACT Caspases are proteases involved in cell death, where caspase-3 is the chief executioner that produces an irreversible cutting event in downstream protein substrates and whose activity is desired in the management of cancer. To determine such activity in clinically relevant samples with high signal-to-noise, plasmon rulers are ideal because they are sensitively affected by their interparticle separation without ambiguity from photobleaching or blinking effects. A plasmon ruler is a noble metal nanoparticle pair, tethered in close proximity to one another *via* a biomolecule, that acts through dipole—dipole interactions and results in the light scattering to increase exponentially. In contrast, a sharp decrease in intensity is observed when the pair is confronted by a large interparticle distance. To align the mechanism of protease activity with building a sensor that can report a binary signal in the presence or absence of caspase-3, we present a caspase-3 selective plasmon ruler (C3SPR) composed of a pair of $Zn_{0.4}Fe_{2.6}O_4$@SiO_2@Au core—shell nanoparticles connected by a caspase-3 cleavage sequence. The dielectric core ($Zn_{0.4}Fe_{2.6}O_4$@SiO_2)-shell (Au) geometry provided a brighter scattering intensity *versus* solid Au nanoparticles, and the magnetic core additionally acted as a purification handle during the plasmon ruler assembly. By monitoring the decrease in light scattering intensity per plasmon ruler, we detected caspase-3 activity at single molecule resolution across a broad dynamic range. This was observed to be as low as 100 fM of recombinant material or 10 ng of total protein from cellular lysate. By thorough analyses of single molecule trajectories, we show caspase-3 activation in a drug-treated chronic myeloid leukemia (K562) cancer system as early as 4 and 8 h with greater sensitivity (2- and 4-fold, respectively) than conventional reagents. This study provides future implications for monitoring caspase-3 as a biomarker and efficacy of drugs.

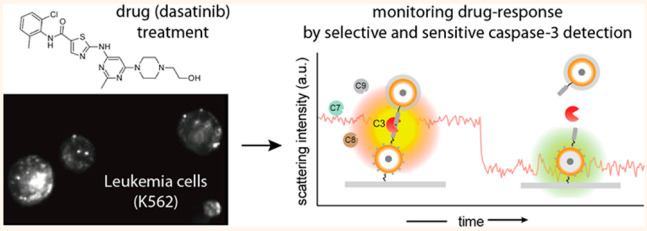

KEYWORDS: caspase · gold nanoparticles · plasmon coupling · leukemia · single molecule

Caspases are a family of proteases that carry out programmed cell death. They are enzymes whose fundamental response is guided by their active site specificity to irreversibly sever a protein substrate[1] and display an exquisite preference to cleave C-terminally to aspartic acids.[2] Two major routes to their activation include (1) the extrinsic or death receptor-induced pathway and (2) the intrinsic or Apaf-1 (apoptotic protease-activating factor-1) apoptosome pathway.[3] The former route is activated through the initiator, caspase-8, while the latter is activated *via* caspase-9. These two pathways converge in their activation of the principal executioner, caspase-3, that perpetrates the downstream hallmarks of apoptosis (degradation of intracellular proteins, nuclear condensation, cell shrinkage, membrane blebbing, and DNA fragmentation).

Assessing caspase-3 activity can be a useful prognosis modality in predicting patient response to pro-apoptotic cancer drugs.[4,5] Provocation from a proapoptotic drug can elicit the signals for cellular destruction as a welcome consequence of chemotherapeutic intervention. However, some cancers have very low caspase-3 activity, which is beyond the detection limits of traditional caspase-3 assays. For example, chronic myeloid leukemia (CML) contained

* Address correspondence to yjun@ohns.ucsf.edu, charles.craik@ucsf.edu.

Received for review May 31, 2014 and accepted August 28, 2014.

Published online August 28, 2014
10.1021/nn502959q

approximately an order of magnitude lower caspase-3 activity, resulting from increased endogenous caspase inhibitors (XIAP and FLIP) and decreased levels of Apaf-1.[6−8]

Traditionally, fluorescence-[2,9−12] or luminescence-based[13,14] techniques have been widely used to detect caspase-3 activity. However, in a system with very low caspase-3 activity, evaluation of drug response requires a higher order of sensitivity than these traditional methods allow.[15] Particularly, in cases where real-time observation over a long time period (>10 min) with single molecule sensitivity is necessary to detect enzymatic reactions with slow kinetics, photobleaching and blinking of fluorophores can be problematic in the interpretation of single molecule data. As an alternative method, plasmon rulers that use interparticle distance-dependent plasmon coupling in a nanoparticle assembly have been demonstrated for sensing DNA hybridization,[16] enzymatic reactions,[17,18] and membrane protein assemblies.[19] We previously reported a crown nanoparticle plasmon ruler that detects caspase-3 activity *in vitro* and *in vivo* through the principle of plasmon coupling, where caspase-3 cleaves a peptide substrate that links a core and satellite plasmonic particles sequentially, causing decoupling of plasmon resonance between the particles.[18] Due to the unique properties of plasmon rulers, including assembly dependent plasmon resonance, strong optical light scattering, and extremely photostable characteristics, highly sensitive detection of caspase-3 activity in a cultured cell line was possible.[18,20−23] We envisioned use of this concept for monitoring drug-response in a more clinically relevant setting by using the CML model system. To realize this in an optimized setting, we designed a new plasmon ruler assay with distinct features from the previous crown nanoparticle plasmon ruler experiments. First, to simplify synthesis, purification, and data analyses, we adopted a dimeric structure consisting of magneto-plasmonic nanoparticles instead of multiparticle assemblies. The relatively large size, complicated purification processes, and heterogeneity in the assembly of crown nanoparticles caused poor colloidal stability, low-throughput production, and massive data analysis, respectively. These characteristics limited their capability as a prognosis tool. The new design resolves these issues where the smaller size, magnetic-purification capability, and defined number of the caspase substrate per ruler allows facile, reproducible, and faster activity analysis.

Second, the new plasmon ruler was designed to have improved caspase-3 selectivity. Traditional caspase-3 activity assays, including the crown nanoparticle plasmon rulers, showed significant cross-reactivity with other caspases (*e.g.* -7, -8, -9), which perturb accurate evaluation of caspase-3 activity of cells treated with drugs. Previous conventional peptide substrates use DEVD-G (P4 to P1′) to detect both caspase-3 and -7 activities.[9,10] A systematic assessment of substrate selectivity uncovered that caspase substrates can be cleaved by multiple caspases.[24] To resolve the individual caspase-3 mediated events among the parallel and consecutive protein signaling networks of an apoptotic cell, a selective imaging tool is required for distinguishing this activity.

Third, we applied the new ruler for prognosis purposes to analyze CML lysates with high sensitivity instead of single cell imaging. Because of their inadequacy for dark-field microscopic imaging arising from CML characteristics (*i.e.* suspension cells) and requirements of ensemble information for prognosis, cell lysate analyses are more desirable than live cell imaging. Such a tool is three-pronged with the following characteristics: (1) exclusivity in detecting caspase-3 as a reliable measure of apoptosis due to its positioning in the cell death cascade, (2) relevance for interrogating drug response in clinical *ex vivo* CML samples where caspase-3 activity is weak, and (3) sensitivity for assaying minimal sample compared to proteomics efforts that require large amounts of cells (Figure 1).

RESULTS

In contrast to the solid Au nanoparticles used previously,[18] the format described here utilizes $Zn_{0.4}Fe_{2.6}O_4$@SiO_2@Au core−shell nanoparticles whose development has been pioneered by the Haus and Halas groups[25−27] and have been favored for their higher extinction coefficients and large optical cross sections.[23] By implementing core−shell nanoparticles, we present a caspase-3 selective plasmon ruler (C3SPR) composed of 50 nm nanoparticles with a 12 nm $Zn_{0.4}Fe_{2.6}O_4$ magnetic core, intermediate SiO_2 layer, and Au shell ($Zn_{0.4}Fe_{2.6}O_4$@SiO_2@Au) (Figure 1). Two improvements were employed to retain a bright signal comparable to the crown nanoparticles while refining issues of heterogeneity, colloidal stability, and selectivity for improved detection of caspase-3 activation. First, $Zn_{0.4}Fe_{2.6}O_4$@SiO_2@Au core−shell nanoparticles provide a ∼3-fold higher scattering intensity above that of solid Au nanoparticles under dark-field microscopy (Supporting Information Figure 1A,B). C3SPRs were constructed in a dimer configuration, where the magnetic core served as a purification handle during dimer synthesis. This increased the proportion of a single species upon its assembly (75% dimer/25% trimer) (Figure 1, Supporting Information Figure 1C). The dimer is held together by Au−thiol and biotin−avidin interactions, while the central peptide sequence is flanked by polyethylene glycol (PEG) spacers (Supporting Information Scheme 1). By simplifying the format from crowns to dimers, colloidal stability is improved due to a decrease in van der Waals interactions between the tethered nanoparticles. Thus, incidence of aggregation is reduced, colloidal stability is heightened, and their

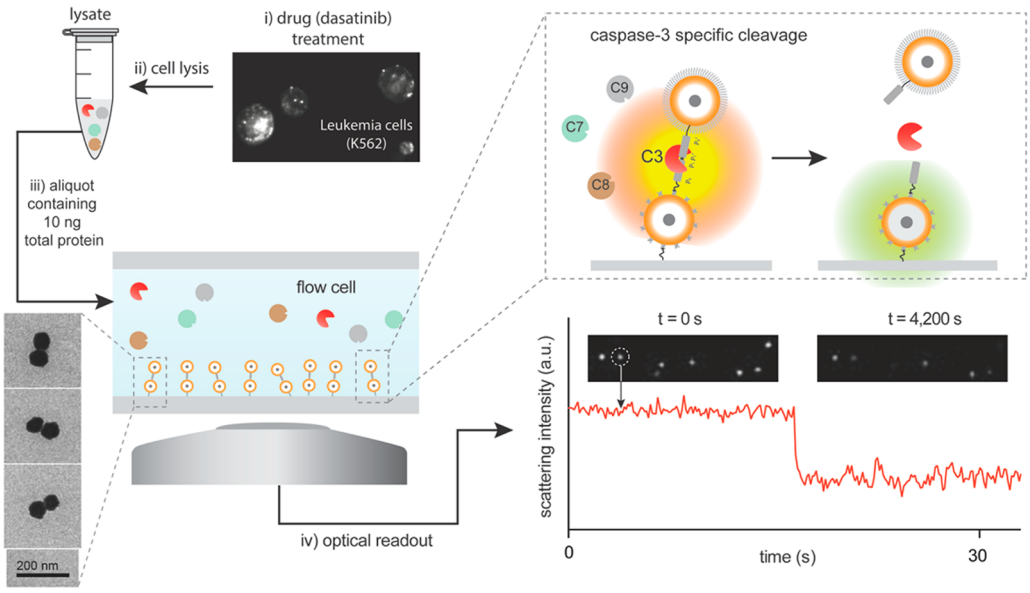

Figure 1. Caspase-3 selective plasmon ruler (C3SPR) for reporting single molecule caspase-3 activity in clinically relevant patient samples. (i) Dark-field microscopy image of CML cells treated with dasatinib. (ii) Cells can be prepared as a lysate and (iii) 10 ng of total protein can be applied to C3SPRs immobilized on a flow chamber for sensitive detection of caspase-3 activity. (Lower left) TEM images following synthesis of the C3SPRs and gel purification. (Upper right) Illustration of a peptide-linked C3SPR with a selective sequence for caspase-3. The selective peptide sequence is depicted in gray from P4 to P1, the scissile peptide bond, and then P1′ to P4′. The intact C3SPR scatters an intense red color. In the presence of caspase-3, the protease cleaves the peptide sequence at the P1−P1′ site. This increases the interparticle distance and the scattering color becomes dim green. (iv) (Above) Optical readout of dark-field microscopy images of caspase-3 treated dimers over time. A representative single particle trace of the C3SPR upon treatment with 1 nM caspase-3. Illustrations not drawn to scale.

ease of use is ensured for further interrogation of protease activity in biological preparations.

To achieve increased selectivity and reduce cross-reactivity with other caspases, we created a protease sensor with a peptide sequence exploiting both non-prime and prime side subsite preferences for caspase-3. The family of caspases (and granzyme B) is partial to cleaving C-terminally to aspartic acids.[2] Fluorogenic substrates from positional scanning synthetic combinatorial libraries (PSSCL) have revealed the nonprime side (P4 to P1) amino acid preferences among the caspases,[2] while both caspase-3 and caspase-7 share an optimal cleavage sequence of DEVD (P4 to P1). Therefore, we first synthesized fluorescent-based substrates by varying the amino acid preferences at the prime side, subjected the peptides to activity assays against a number of caspases (Figure 2A), and their kinetic parameters were obtained (Supporting Information Table 1 and Supporting Information Figure 2).

The substrates consist of an 8-mer peptide (P4 to P4′) flanked by a donor/quencher pair, 7-methoxycoumarin/dinitrophenol (Lys-MCA/Lys-DNP). With the crown nanoparticles, DEVD-**G**GSN was the critical 8-mer sequence utilized for caspase-3 detection.[18] DEVD-**G** has been used in previously published caspase reporters[9,10] and Stennicke *et al.*[11] describe a general preference for small amino acids, like glycine, in the P1′ position. However, charged residues are prohibited and this quality has been exploited by Albeck *et al.*[12] and in this present work to increase selectivity for caspase-3 over other caspase family members. Stennicke *et al.*[11] prepared shorter 7-mer peptides (P4 to P3′) flanked by a Gly-Abz and Asp-NO_2 pair. They observed that a change in the P1′ residue from G to R brought about a reduction in the catalytic efficiency with caspase-3, while increasing its selectivity over that of caspases 7 and 8. When this single substitution in our fluorescent substrates was made, a remarkable increase in selectivity for caspase-3 became apparent with peptides, (2) DEVD-RGSN, (3) DEVD-RVYG, and (4) DEVD-RVYD, showing little or no activity against caspase-7 (Figure 2A and Supporting Information Figure 2). Furthermore, activity when treated with caspase-8 was greatest among peptides, (1) DEVD-GGSN and (4) DEVD-RVYD, while activity was absent among all the DEVD-containing peptides when treated with caspase-9. Two additional peptides were tested that recognized granzyme B activity, but caspases 3 and 7 did not display such a response (Supporting Information Table 1).

With regard to selectivity (Supporting Information Figure 2), (2) DEVD-**R**GSN was 49-fold selective for caspase-3 compared to only a 9-fold increase in selectivity when P1′ Gly is retained. When additional determinants were altered, (3) DEVD-RVY**G** and (4) DEVD-RVY**D** were >760- and >312-fold more selective for caspase-3, respectively. Assessment of favorable caspase-3 selectivity over that of caspase-8 follows

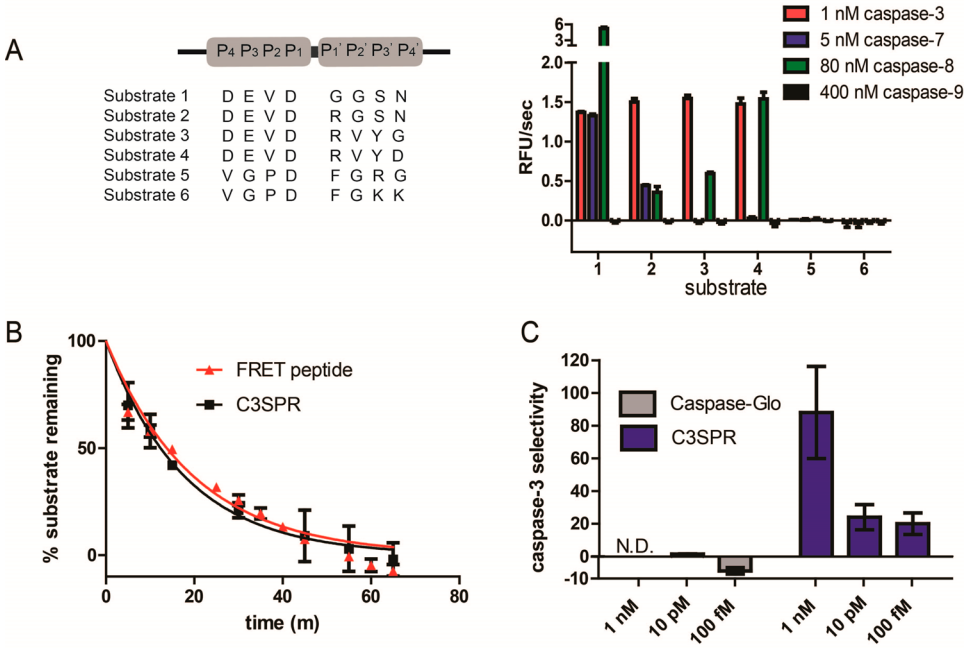

Figure 2. Selectivity of the plasmon rulers for detecting caspase-3 activity. (A) (Left) Peptide sequences of FRET substrates were synthesized. Peptides were flanked by methoxycoumarin and dinitrophenol donor/quencher pairs (not shown). (Right) Caspase activity assay among fluorescent peptides. The 30 μM peptides were assayed against 1 nM caspase-3 (red), 5 nM caspase-7 (blue), 80 nM caspase-8 (green), and 400 nM caspase-9 (black). Activities reported are from the first 1500 s of the linear portion of the progress curve. (B) Comparison of C3SPR and FRET peptide, both containing DEVD-RVYG. Percent substrate remaining against time upon exposure to 1 nM caspase-3. Catalytic efficiencies (FRET peptide, 840 000 M^{-1} s^{-1}; C3SPR, 940 000 M^{-1} s^{-1}) were calculated using a first-order exponential decay function. (C) Selectivity was determined from the ratio of caspase-3 activity over caspase-7 activity using Caspase-Glo (gray) or ratio of product generated upon treatment with caspase-3 over -7 using C3SPRs (purple). Data presented in (B) and (C) were background subtracted (Supporting Information Figures 3 and 4). N.D. = not determined.

the trend: (2) DEVD-RGSN > (3) DEVD-RVYG > (4) DEVD-RVYD > (1) DEVD-GGSN (771 > 760 > 312 > 61). Selectivity for caspase-3 relative to caspase-9 is above the levels displayed previously for caspase-8. These results suggest that DEVD-RVYG (substrate 3) is the optimal sequence to be installed into the plasmon ruler construct. Furthermore, these enhancements ensure the future utility of these C3SPRs to detect caspase-3 activation in other cancer systems that express both caspase-3 and -7. It is noted that the concentrations used in the caspase activity assay (Figure 2A, right) were selected as in the literature.[11,28] Additionally, there is a higher concentration of initiator caspases *versus* executioner caspases in apoptotic cells.[29] Thus, excess concentrations of initiator caspases were used to ensure caspase-3 selectivity.

To test whether a change in scattering signal to the protease sensor construct will directly measure caspase-3 activity, C3SPRs were immobilized onto a glass flow chamber to report caspase-3 kinetics (Figure 1). Under dark-field microscopy, the C3SPRs responded to treatment with 1 nM caspase-3 by displaying a decrease in scattering intensity over the duration of the experiment (Figure 1, Supporting Information Figure 5). Each C3SPR's scattering intensity was recorded at 10 Hz and provided a trajectory indicating the time at which caspase-3 produced a cutting event (Figure 1). The number of cutting events observed was enumerated into 5 min bins, where 28% of the cutting events were generated at the onset of the experiment (Supporting Information Figure 6). By monitoring the % substrate remaining, we found that the k_{cat}/K_M value measured from the dimers (940 000 M^{-1} s^{-1}) was within the same order of magnitude (1.1-fold difference) as the DEVD-RVYG-containing fluorescent peptide (840 000 M^{-1} s^{-1}), thus making the dimer a reliable sensor for caspase-3 detection (Figure 2B). Meanwhile, treatment of the optimized sensor with 5 nM caspase-7 delivered minimal cutting events over a 1.5 h duration (Supporting Information Figure 7). To further challenge the selectivity and sensitivity of the C3SPRs, caspase-3 was titrated to establish the dynamic range of this nanoparticle sensor against a conventional luminescent reagent (Caspase-Glo 3/7 Assay Systems, Promega). Briefly, Caspase-Glo 3/7 Assay Systems utilize a DEVD-containing substrate that becomes luminescent upon exposure to either caspase-3 or -7. The cleavage product, aminoluciferin (substrate of luciferase), is the component of the assay that generates the luminescent readout that is proportional to caspase-3/7 activity. The format of the assay is done in multiwell plates where a 1:1 ratio of the Caspase-Glo 3/7 reagent is applied to either recombinant caspase or cell culture treatments. After a kinetic run, Caspase-Glo

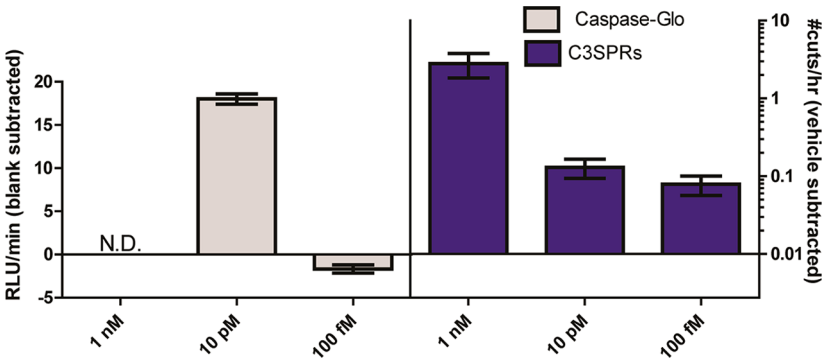

Figure 3. Sensitivity of C3SPRs to traditional caspase assay. (Left) Optimal concentration range of caspase-3 detection *via* Caspase-Glo 3/7 after a kinetic run was in the picomolar range. One nanomolar caspase-3 produced no fit and was outside of the dynamic range of the luminescence assay. (Right) Activity was determined by measuring no. of cuts per unit time when 100 fM, 10 pM, or 1 nM caspase-3 was assayed against a platform of C3SPRs during a kinetic run at single molecule resolution. Values were calculated from the linear portion of the progress curves.

3/7 detected recombinant caspase-3 and -7 in the picomolar range, while detection of 1 nM caspase-3/7 was outside of the reagent's dynamic range (Figure 3 gray bars, and Supporting Information Figure 8). Overall, caspase-3 selectivity was marginal at 10 pM with a 1.5-fold increase in selectivity for this principal executioner caspase (Figure 2C, gray bars). With the C3SPRs, 100 fM, 10 pM, and 1 nM caspase-3 were readily detected above caspase-7 conditions (Figure 2C, purple bars) and single molecule imaging was apparent with as little as 100 fM caspase-3 exposure (Figure 3, purple bars). Selectivity observed with 100 fM, 10 pM, and 1 nM caspase-3 treatment against the C3SPRs displayed a 20-, 24-, and 90-fold increase above caspase-7, respectively (Figure 2C, purple bars). These values rival those observed when the Caspase-Glo 3/7 assay system was employed. Thus, the C3SPRs have a broader dynamic range spanning the 100 fM to 1 nM concentration range, while selectivity for caspase-3 is ensured during a time course. Taken together, these results suggest that the sensors are highly effective in reporting caspase-3 activity.

To assess early cell death in cells that have been challenged with the clinically approved kinase inhibitor dasatinib, we utilized the chronic myeloid leukemia cell line K562 as a model system due to its demonstrated pro-apoptotic activity.[30] In evaluating the success of performing single molecule imaging experiments on K562 suspension cells containing sensors, we found that the conditions were not ideal (Supporting Information Movie 1) even when restrained with poly-L-lysine, concanavalin A, DNA methods, or antibody conjugation to cell surface marker CD71 (data not shown). Their smaller dimensions (~20 μm) also prevented a high distribution of C3SPRs within each cell for statistically significant quantification of caspase-3 mediated events. Therefore, we chose to proceed with interrogation of K562 cellular lysates.

First, activity in lysate prepared from 24 h dasatinib treated K562 cells was detectable in the range of 0.1 μg to 1 μg total protein *via* Caspase-Glo 3/7 with a signal-to-noise ratio from ~3.5 to 4-fold, while caspase-3/7 activity was difficult to observe in the 8 h dasatinib treated regimen across the total protein concentrations assayed (Figure 4A). In contrast, the C3SPRs sensitively responded to activity in 10 ng K562 lysate, where the cells were exposed to dasatinib for 4 and 8 h prior to lysate preparation (Figure 4B and Supporting Information Figure 9). Sensitive detection was observed ~2-fold and 4-fold above vehicle conditions, respectively, while the 100 μM z-DEVD-cmk caspase-3 inhibitor control resulted in minimal cutting events *versus* the DMSO control. Meanwhile, a ~5-fold increase in cutting events was observed in the chamber treated with 10 ng lysate from 24 h dasatinib treated K562 cells (Figure 4B). As only 10 ng of total protein was applied to each platform of nanoparticles, this translates to activity contained within ~55−65 cells being interrogated at single molecule resolution. As a comparison, Western blotting methods utilizing 10 μg total protein/well equates to ~55 000−65 000 cells needed for assessing activity,[31] while flow cytometry methods require ~500 000 cells per experimental group.[30] This promises high-throughput and highly sensitive diagnosis capabilities in microfluidic applications. In the present study, we used a custom-made chamber with a 50 μL channel volume, but further reduction of sample volume down to 1 μL (which corresponds to the total protein in a single CML cell at the concentration used, see Materials and Methods) may be easily accommodated by using a conventional microfluidic geometry. Furthermore, cutting event analyses could also be done by simply comparing two dark-field images before and after treatment of caspase-3, where a single cutting event occurs when the scattering intensity in the final frame is less than or equal to half of the initial scattering intensity in the first frame. We confirmed that counting the cutting events *via* this process (Figure 4B) *versus* inspection of entire single particle trajectories[15,18] provided the same results (Supporting Information Figure 10).

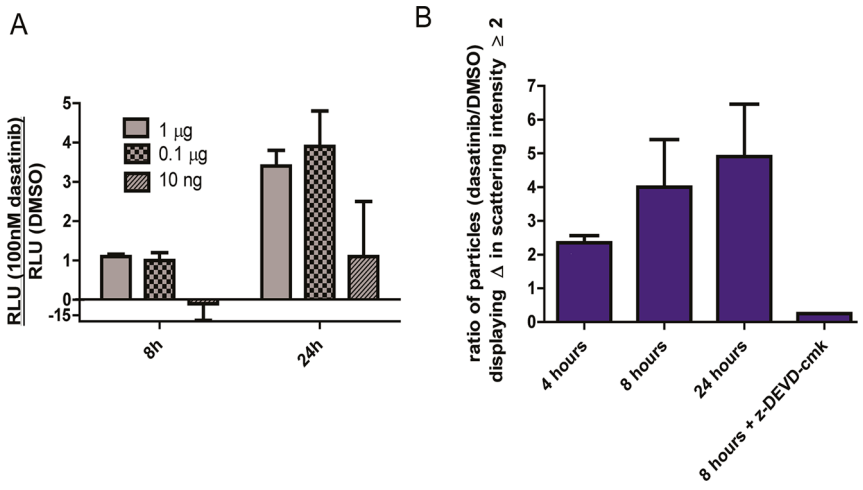

Figure 4. Sensitive detection of caspase-3 activity from dasatinib and DMSO treated K562 cell lysates using C3SPRs. (A) Signal-to-noise ratio of RLU generated in the presence of 100 nM dasatinib over DMSO using Caspase-Glo 3/7 in 8 and 24 h treated samples assayed at different total protein concentrations. (B) Drug treated lysate *versus* vehicle control using C3SPRs. Signal-to-noise ratio of particles displaying a change in scattering intensity greater than or equal to 2 after 80 min, with background subtraction. Ten nanograms of total protein was applied per chamber for 4, 8, and 24 h time points. Ten nanograms total protein corresponds to the cellular material contained within ~55–65 CML cells.

CONCLUSIONS AND DISCUSSION

In conclusion, C3SPRs were constructed with a pair of $Zn_{0.4}Fe_{2.6}O_4$@SiO_2@Au core–shell nanoparticles to offer a simpler construct to decrease heterogeneity in its synthesis and increase colloidal stability for prolonged experimental use. Selectivity for caspase-3 detection was accomplished by tuning the P1′ residue to establish exclusive observation of caspase-3 mediated events. This allows for easy carryover to other cancer systems that are of biological interest. The C3SPRs permitted observation of recombinant caspase-3 activity in as little as 100 fM with high signal-to-noise, which was not detectable by Caspase-Glo 3/7. It is noted that the caspase-3 titration using the C3SPRs produced k_{cat}/K_M values values greater than expected and such kinetics under these nanoparticle conditions is currently under further investigation.

In fact, previous observations of enhanced activity with nanoparticle–substrate conjugates are prevalent in literature and have generated much interest.[32−38] In fact, Algar *et al.* propose a "hopping" mode to explain the elevated trypsin activity observed at the multivalently functionalized quantum dot (QD)–peptide interface.[33] They observed an initial rate enhancement with consumption of the high local concentration of substrates before translocation (*i.e.*, hopping) of the protease elsewhere. This has also been documented with regard to nuclease activity on Au-oligonucleotide conjugates.[37] Algar *et al.* assert that the protease and nanoparticles are involved in weak collisional associations, where affinity for the PEGylated surface also contributes to these productive interactions. In fact, PEG has been documented to promote weak and reversible contacts with proteins.[39−41] As hypothesized by Tassa *et al.*[34] and You *et al.*,[36] complex interactions between the nanoparticle surface with proteins and contributions from hydrophobicity, polarity, and charge greatly influence the binding events observed between these discrete entities, though our understanding of these determinants is still incomplete. Favorable electrostatic interactions, along with the PEGylated surface, that draw caspase-3 to the nanoparticle interface may have an influence on the enhanced kinetics that we report.

Furthermore, the C3SPRs sensitively responded to activity in a CML cancer cell line known to be hindered by endogenous caspase inhibitors that could limit observation of caspase-3 activity using conventional techniques. This was evident in as little as 10 ng total protein in 4 and 8 h drug treated K562 cell lysates, which is more sensitive than the proprietary luminescent reagent. The amount of total protein corresponds to tens of cells compared to the thousands of cells required for conventional Western blotting or flow cytometry methods. The observations made here support an early commitment to apoptosis that precedes the competing fate of growth factor mediated survival in CML patient-derived cells.[31] Our highly sensitive and selective nanoparticle tool directly reported caspase-3 activity in drug treated cell lysates as a dependable apoptotic marker. Such a nanoparticle tool has further implications in observing caspase-3 as a relevant biomarker in a clinical sample before pathogenic changes occur at the anatomical level. As a downstream application, one can imagine capturing the cellular contents of single cells using the method developed by Lim and Abate,[42] followed by application of the cellular material to the C3SPRs, and a final sorting component of protease activity on a microfluidics platform with high-throughput capabilities. With the additional

improvements to our high-throughput data analysis (see Materials and Methods), parsing of nanoparticle responses that are of immediate interest become readily apparent. Subsequent analysis of whole single particle trajectories can be performed to extract kinetic data. Indeed, implications for use in microfluidic devices and drug screening can be envisioned for the personalized treatment of cancer.

MATERIALS AND METHODS

Fluorescent Peptide and Linker Synthesis. Fluorescent peptides and linkers were synthesized *via* standard solid phase peptide synthesis protocols. Rink amide resin (Rink resin SS, 100-200 mesh, Advanced Chemtech) was used to prepare peptide amides, while 2-chlorotrityl chloride resin (Novabiochem) was used to synthesize the nanoparticle linkers. Fmoc-protected amino acids, Fmoc-Lys(Mca)-OH, Fmoc-Lys(Dnp)-OH, Fmoc-PEG$_{20atoms}$-OH, Fmoc-PEG$_{40atoms}$-OH, PyBop, and HOBt, all used at 3 equiv per reaction, were purchased from Novabiochem. Dichloromethane (DCM), dimethylformamide (DMF), piperidine (used as 20% in DMF), diisopropylethylamine (DIPEA, used at 4.5 equiv per reaction), trifluoroacetic acid (TFA), triisopropylsilane (TIPS), ethanedithiol (EDT), diethyl ether, and acetonitrile (ACN) were used as received. Acetic anhydride and pyridine were purchased from Sigma. The central 8-mer residues of each peptide were coupled using a Symphony Quartet peptide synthesizer (Protein Technologies), while all other moieties were coupled manually. Acetylation was completed under conditions of acetic anhydride/pyridine/DMF (1:2:3) for 1 h, while biotinylation was performed with EZ-Link NHS-Biotin (Thermo Scientific) used at 1.5 equiv per reaction. Couplings and deprotection were confirmed by the Kaiser test. Peptides were cleaved under 95% TFA/2.5% TIPS/2.5% H_2O or 94% TFA/2.5% H_2O/2.5% EDT/1% TIPS (for Cys-containing linkers) conditions and precipitated into cold ether. Purification was done on an Agilent 1200 series system with a C18 reverse phase column (Waters). Mobile phase consisted of 99.9% H_2O/0.1% TFA (solvent A) and 95% ACN/4.9% H_2O/0.1% TFA (solvent B). Characterization was performed on an LC−MS on a Waters Alliance liquid chromatography system with a Waters Micromass ZQ single-quadrupole mass spectrometer. Fluorescent peptides were protected from light as appropriate.

Enzyme Assays. All peptides were dissolved in a minimal volume of DMSO (Sigma #S6942) and Ac-Lys(Dnp)-DEVD-GGSN-Lys(Mca)-NH_2 and Ac-Lys(Dnp)-VGPD-FGRG-Lys(Mca)-NH_2 were submitted for amino acid analysis (Texas A&M University, Protein Chemistry Laboratory, Department of Biochemistry). Total hydrolysis of all six fluorescent peptides was performed in the presence of either 100 nM caspase-3 or 100 nM granzyme B in triplicate. Caspase buffer contained 10 mM PIPES, 0.1 M NaCl, 0.1 mM EDTA, 10 mM DTT, 10% (w/v) sucrose, and 0.1% CHAPS, pH 7.2,[11,28] while granzyme B buffer included 50 mM NaHEPES pH 8, 100 mM NaCl, and 0.01% Tween-20. Incubation was performed overnight at 37 °C. After 24 h, samples were read on a Microfluor 1 black plate (Thermo #7005, U bottom) and an end point reading was monitored from the emission at 393 nm upon excitation at 328 nm using a Gemini EM fluorescence plate reader. Peptide concentration was determined from the final fluorescence of totally hydrolyzed Ac-Lys(Dnp)-DEVD-GGSN-Lys(Mca)-NH_2 or Ac-Lys(Dnp)-VGPD-FGRG-Lys(Mca)-NH_2 as standards.

Catalytic parameters were determined at initial peptide concentrations from 3 to 30 μM in the presence of caspase-3, -7, -8, -9 (kindly provided by Prof. James Wells and Dr. Julie Zorn, UCSF) or starting peptide concentrations from 3 to 90 μM in the presence of 10 nM granzyme B. As in ref 11, 2 μL of peptide was combined with 98 μL of buffer containing the enzyme of interest.[28] Fluorescence (emission 393 nm/excitation 328 nm) was monitored during a 2 h kinetic run. The initial slope was obtained from the linear portion of the progress curve and plotted against the initial peptide concentrations. To yield the k_{cat} and K_M parameters, this was fit to the Michaelis−Menten equation in Kaliedograph software. Four replicates were run per assay. The % substrate generated *versus* time figure was plotted in GraphPad Prism 5 and fitted using a first-order exponential decay model. Data was constrained using the parameters: plateau = 0 and *Y* (initial) = 100 with a robust fit.

K562 Lysate Preparation. K562 cells were maintained in RPMI 1640 medium supplemented with 10% FBS, 1× L-glutamine, and 1× penicillin/streptomycin as in the literature.[30,31] Briefly, cells were seeded at 2 × 10^5 cells/mL in a T-75 flask. Cells were induced with dasatinib or vehicle. At the end of each time point, cells were pelleted at 2500 RCF for 5 min. Supernatant was discarded. Pellets were washed 2× with cold PBS, with spinning in between washes at 2500 RCF for 5 min. Pellets were removed entirely of PBS. Lysis buffer contained 50 mM HEPES pH = 7.4, 1% Triton X-100, 0.1% CHAPS, 1 mM DTT (added fresh), and 0.1 mM EDTA supplemented with protease and phosphatase inhibitors diluted at 1:100 (Calbiochem #539134 and #524625, respectively). Lysis buffer was added to each pellet and kept on ice with intermittent flicking for 15 min. Pellets were spun at 14 000 RCF for 15 min at 4 °C. Supernatant was transferred to new tubes and protein concentrations were determined by BCA Protein assay (Thermo Scientific #23227). Lysates were aliquoted, flash frozen in liquid nitrogen, and stored at −80 °C.

Caspase-Glo 3/7 Assay. Methods were followed according to the manufacturer's instructions. Briefly, caspase-3 and -7 were prepared as stocks between 200 fM and 2 nM in caspase buffer. Lysates were prepared as stocks between 10 ng and 1 μg total protein in caspase buffer supplemented with protease and phosphatase inhibitors diluted at 1:100 (Calbiochem #539134 and #524625). Stock solutions (100 μL) were diluted with 100 μL of Caspase-Glo 3/7 proprietary reagent. Assay was conducted in triplicate in a 96-well solid white plate (E&K Scientific, #EK-25075) on a SPECTRAmax plate reader. Data points were blank subtracted.

Caspase-3 Selective Plasmon Ruler (C3SPR) Synthesis. Magnetic Au nanoparticles were synthesized through sequential growth of SiO_2 and then Au on a 12 nm $Zn_{0.4}Fe_{2.6}O_4$ nanoparticle.[43,44] Briefly, we first performed amine-functionalized silica coating on the magnetic nanoparticles *via* a water-in-oil immersion method reported by Yi *et al.*[45] Separately, gold nanoclusters were prepared by the Baiker method.[46] The gold cluster solution was mixed with the magnetic-silica nanoparticle solution, and was allowed to react for another 7 h. The resulting magnetic-silica/Au core/satellite nanoparticles were purified *via* a midi MACS column (Miltenyi Biotec) with 10 mM Tris pH 8.0 (T0). Gold shells were further formed by the reduction of gold precursors, and this reaction was modified from those of Weiser and Duff *et al.*[47,48] The resulting magnetic Au nanoparticles were purified by centrifugation, and a midi MACS column. Detailed synthetic procedures will be published elsewhere.[49]

Thiols were reduced by treatment of 10 pmol biotin-PEG$_{20atoms}$-DEVD-RVYG- PEG$_{60atoms}$-CCC-COOH or 10 pmol biotin-PEG$_{60atoms}$-CCC-COOH with 10 nmol bis(*p*-sulfonatophenyl)-phenylphosphine dihydrate dipotassium salt (BSPP, Strem Chemicals, 1000× molar excess) in separate tubes. Volume was brought up to 20 μL using 10 mM Tris pH 8.0. Both tubes were applied to a shaker for 10 min.

The 0.4 pmol magnetic Au core/shell nanoparticles (50 nm diameter) were washed with 5 column volumes of H_2O using a midi MACS column and eluted. Alternatively, they can be spun at 1000 RCF for 7 min and washed with H_2O (3×). Magnetic Au nanoparticles were concentrated to 0.5 nM. Reduced peptide or PEG linker solutions above were added to 0.2 pmol magnetic Au nanoparticles under 10 mM citrate pH 3 conditions[50] for 20 min with shaking. Reaction was quenched with H_2O and washed with 5 column volumes of H_2O using a midi MACS column and eluted in 10 mM Tris pH 8.0 with 30 mM NaCl (T30). Conjugated

magnetic Au nanoparticles can alternatively be washed with H_2O *via* centrifugation, as mentioned above, and dispersed in T30. Conjugated magnetic Au nanoparticles were concentrated to 0.5 nM. It is noted that a 50-fold molar excess (Supporting Information Figure 11) of peptide linkers was applied to the nanoparticles during conjugation. The number of peptides was determined by conjugating them with a large excess of streptavidinylated quantum dots for screening purposes. The number of quantum dots attached was monitored by agarose gel electrophoresis by line profiling analyses (ImageJ). At 50-fold molar excess, the number of peptides per nanoparticle was estimated around 1−8. Following subsequent gel purification steps of higher order species, this ratio gave the most effective yield of dimers as shown in our TEM images and statistics. Though we note that our peptide-conjugated nanoparticles are likely functionalized with more than a single peptide (*ca.* 1−8) with surrounding PEG moieties (Supporting Information Scheme 1 and 2), any peptides functionalized with only a single magnetic Au nanoparticle are "invisible" peptides whose response is not observed *via* scattering intensity during the nanoparticle assays.

A volume of 40 nmol HS-$C_{11}EG_6$-COOH (2×10^5 molar excess, Prochimia) was added to each aliquot of nanoparticles and the mixtures were shaken overnight at room temperature (RT). A mini MACS column was used to remove unreacted HS-$C_{11}EG_6$-COOH by washing with five column volumes of T30. Each set of nanoparticles was eluted from the column or underwent repeated centrifugation as mentioned above. PEG conjugated nanoparticles were modified using 2 nmol filter sterilized streptavidin (Stv) in T30 and shaken for 1 to 2 h. Stv-PEG conjugated nanoparticles were washed with five column volumes of 10 mM Tris pH 8.0, 0.04% PEG 8000 on a mini MACS column. Stv-PEG conjugated nanoparticles were eluted from the column or underwent repeated centrifugation as mentioned above. Peptide and Stv-PEG conjugated nanoparticles were added in a 1:1 ratio to form dimers. Filter sterilized 1 M NaCl was added dropwise to give a final concentration of 60 mM NaCl and the mixture shook overnight at RT. C3SPRs were separated *via* electrophoresis in a 0.7% agarose gel with 0.5× TBE buffer. Gel was run at 100 V for 30 min. Dimers were isolated by cutting the appropriate band out of the gel, placing it into a dialysis bag containing T30 buffer, and running the dialysis bag in the electrophoresis chamber containing 0.5× TBE buffer. C3SPRs were characterized on a Phillip Tecnai G^2 20 transmission electron microscope.

Single Molecule Imaging of Caspase-3 Activation. Flow chambers were prepared using the procedures mentioned in.[15,51] Briefly, four holes were drilled through a glass slide using a 0.75 mm diamond drill bit. Glass slides and coverslips (24 × 60) were sequentially washed in 5% alconox, H_2O, 1 M KOH, and H_2O with sonication for 20 min in a water bath. Glass was dried using high purity Ar sprayed at 40 psi. Flow chambers were assembled using 3 in. × 3 mm strips of double-sided tape oriented along the length of the glass slide. A coverslip was placed atop the taped areas and sealed using epoxy glue. Chambers were washed with filtered T30, followed by washes with filtered 1 mg/mL BSA−biotin. BSA−biotin was incubated for 10 min and subsequently washed with filtered T30. C3SPR solution was diluted 4-fold using T30. A volume of 50 μL was applied per chamber and the solution was allowed to incubate for 10 min. Unreacted particles were washed with filtered T30. Chambers were further assembled with trimmed pipet tips and needles to serve as inlets and outlets, respectively. Tubing was attached to the needle and connected to a syringe with a needle to serve as a waste reservoir.

Caspase-3 and caspase-7 were diluted in either caspase buffer or PBS. K562 lysates were flash frozen as concentrated stocks at a total protein concentration of ∼6 μg/μL. To minimize exchange of the C3SPR surface with amines, thiols, *etc.*, K562 lysate was diluted in caspase buffer or PBS supplemented with protease and phosphatase inhibitors at a 1:100 dilution (Calbiochem #539134 and #524625) and filtered prior to imaging. These samples were ultimately diluted ∼24 000 times to give a final total protein concentration of 0.25 ng/μL. Microscopy was conducted using an inverted Ti-E Nikon microscope outfitted with a dry dark-field condenser (N.A. 0.95−0.8) or oil dark-field condenser (1.43−1.20), Andor iXon 512 × 512 EMCCD detector, PAXcam color camera, Ti-E Perfect Focus, and Micro-Manager software.[52] Fresh buffer was introduced to the C3SPRs for equilibration, followed by 50 μL of caspase solution or diluted lysate. Acquisition was conducted at 10 Hz and ImageJ or MatLab software was used to obtain scattering intensities of each nanoparticle in the field of view. Single particle trajectories were primarily measured using ImageJ using the method described in Tajon *et al.*[15] and kinetics were analyzed using a first-order exponential decay model in GraphPad Prism 5 (constraints: plateau = 0, *Y* (initial) = 100, robust fit). Contribution of nanoparticle response obtained under vehicle conditions was subtracted from the caspase-3/7 activity observed for the C3SPR experiments.

Analyzing C3SPR Response Using Ratio of Intensities from First and Last Frames. Scattering intensity of C3SPRs in the first frame and last frame were measured. Ten background regions (empty region without particles) were chosen per FOV (1st and last frame). Regions were the same area as those used for particle picking. Average of scattering intensity from background regions was calculated. Particle scattering intensities were background subtracted. Ratio of starting/ending intensities (background subtracted) was calculated. Per experimental condition, ratios equal to or greater than 2 were enumerated and divided by the number of particles analyzed. From these values, the ratio of particles (dasatinib over DMSO treated samples) was determined to give a measure of signal-to-noise.

Conflict of Interest: The authors declare no competing financial interest.

Acknowledgment. C.A.T. was supported as an appointee on the Microbial Pathogenesis and Host Defense Training Grant (T32-GM64337) and received the UCSF Quantitative Biosciences Consortium (QBC) Fellowship and NIGMS-IMSD award (R25-GM56847). D.S. was supported by the Human Frontier Science Program Cross-disciplinary postdoc research fellowship. J.A. received support from the NIH Training Grant T32 GM007175 and the UC Cancer Research Coordinating Committee (CRCC) Fellowship. Y.J. was supported from the National Institute of Biomedical Imaging and Bioengineering and National Institutes of Health (NIH 1R21EB015088). C.S.C received support from the National Institutes of Health (NIH R01CA128765). N. Shah is a Leukemia & Lymphoma Scholar in Clinical Research. We thank J. Wells (University of California, San Francisco) and J. Zorn for providing us with purified recombinant caspases. Mass spectrometry was provided by the Bio-Organic Mass Spectrometry Resource at UCSF (A. Burlingame, Director) supported by the Biomedical Research Technology Program of the NIH National Center for Research Resources (NIH NCRR P41RR001614 and NRCC RR014606). Amino acid analysis was performed at Texas A&M University (Protein Chemistry Laboratory, Department of Biochemistry). The authors thank C. Duan (Boston University) for critical review of the manuscript.

Supporting Information Available: Movie of K562 cells containing C3SPRs and additional figures, schemes, and table on the characterization of C3SPR, caspase-3 selectivity, indirect response of C3SPRs to vehicle treatment, quantification of inactive C3SPRs treated with excess caspase-3, evidence that dimers and cleaved monomeric product are distinguishable under dark-field microscopy *via* scattering intensity, plot of number of cutting events *versus* time upon exposure to 1 nM caspase-3 using C3SPRs, representative single particle trace of a C3SPR after treatment with caspase-7, sensitivity of the Caspase-Glo 3/7 reagent, C3SPR responsiveness to K562 vehicle- and drug-treated lysates, ratio of cutting events observed per K562 lysate condition, gel image of magnetic Au nanoparticle−biotin conjugation with streptavidin−QD at different molar concentrations of peptide, schematics of the C3SPR and how peptide tethers linked to a single nanoparticle do not affect scattering intensity readout, kinetic parameters of FRET peptides. This material is available free of charge *via* the Internet at http://pubs.acs.org.

REFERENCES AND NOTES

1. Farady, C. J.; Craik, C. S. Mechanisms of Macromolecular Protease Inhibitors. *ChemBioChem* **2010**, *11*, 2341–2346.
2. Thornberry, N. A.; Rano, T. A.; Peterson, E. P.; Rasper, D. M.; Timkey, T.; Garcia-Calvo, M.; Houtzager, V. M.; Nordstrom, P. A.; Roy, S.; Vaillancourt, J. P.; *et al.* A Combinatorial Approach Defines Specificities of Members of the Caspase Family and Granzyme B. Functional Relationships Established for Key Mediators of Apoptosis. *J. Biol. Chem.* **1997**, *272*, 17907–17911.
3. Logue, S. E.; Martin, S. J. Caspase Activation Cascades in Apoptosis. *Biochem. Soc. Trans.* **2008**, *36*, 1–9.
4. Meyer, L. H.; Karawajew, L.; Schrappe, M.; Ludwig, W. D.; Debatin, K. M.; Stahnke, K. Cytochrome c-related Caspase-3 Activation Determines Treatment Response and Relapse in Childhood Precursor B-Cell ALL. *Blood* **2006**, *107*, 4524–4531.
5. Estrov, Z.; Thall, P. F.; Talpaz, M.; Estey, E. H.; Kantarjian, H. M.; Andreeff, M.; Harris, D.; Van, Q.; Walterscheid, M.; Kornblau, S. M. Caspase 2 and Caspase 3 Protein Levels as Predictors of Survival in Acute Myelogenous Leukemia. *Blood* **1998**, *92*, 3090–3097.
6. Schimmer, A. D.; Pedersen, I. M.; Kitada, S.; Eksioglu-Demiralp, E.; Minden, M. D.; Pinto, R.; Mah, K.; Andreeff, M.; Kim, Y.; Suh, W. S.; *et al.* Functional Blocks in Caspase Activation Pathways are Common in Leukemia and Predict Patient Response to Induction Chemotherapy. *Cancer Res.* **2003**, *63*, 1242–1248.
7. Jia, L.; Srinivasula, S. M.; Liu, F. T.; Newland, A. C.; Fernandes-Alnemri, T.; Alnemri, E. S.; Kelsey, S. M. Apaf-1 Protein Deficiency Confers Resistance to Cytochrome c-Dependent Apoptosis in Human Leukemic Cells. *Blood* **2001**, *98*, 414–421.
8. Tamm, I.; Kornblau, S. M.; Segall, H.; Krajewski, S.; Welsh, K.; Kitada, S.; Scudiero, D. A.; Tudor, G.; Qui, Y. H.; Monks, A.; *et al.* Expression and Prognostic Significance of IAP-Family Genes in Human Cancers and Myeloid Leukemias. *Clin. Cancer Res.* **2000**, *6*, 1796–1803.
9. Rehm, M.; Dussmann, H.; Prehn, J. H. Real-Time Single Cell Analysis of Smac/DIABLO Release During Apoptosis. *J. Cell Biol.* **2003**, *162*, 1031–1043.
10. Tyas, L.; Brophy, V. A.; Pope, A.; Rivett, A. J.; Tavare, J. M. Rapid Caspase-3 Activation During Apoptosis Revealed Using Fluorescence-Resonance Energy Transfer. *EMBO Rep.* **2000**, *1*, 266–270.
11. Stennicke, H. R.; Renatus, M.; Meldal, M.; Salvesen, G. S. Internally Quenched Fluorescent Peptide Substrates Disclose the Subsite Preferences of Human Caspases 1, 3, 6, 7 and 8. *Biochem. J.* **2000**, *350* (Pt. 2), 563–568.
12. Albeck, J. G.; Burke, J. M.; Aldridge, B. B.; Zhang, M.; Lauffenburger, D. A.; Sorger, P. K. Quantitative Analysis of Pathways Controlling Extrinsic Apoptosis in Single Cells. *Mol. Cell* **2008**, *30*, 11–25.
13. Liu, D.; Li, C.; Chen, Y.; Burnett, C.; Liu, X. Y.; Downs, S.; Collins, R. D.; Hawiger, J. Nuclear Import of Proinflammatory Transcription Factors Is Required for Massive Liver Apoptosis Induced by Bacterial Lipopolysaccharide. *J. Biol. Chem.* **2004**, *279*, 48434–48442.
14. Ren, Y. G.; Wagner, K. W.; Knee, D. A.; Aza-Blanc, P.; Nasoff, M.; Deveraux, Q. L. Differential Regulation of the TRAIL Death Receptors DR4 and DR5 by the Signal Recognition Particle. *Mol. Biol. Cell* **2004**, *15*, 5064–5074.
15. Tajon, C.; Jun, Y. W.; Craik, C. S. Single-Molecule Sensing of Caspase Activation in Live Cells *via* Plasmon Coupling Nanotechnology. *Methods Enzymol.* **2014**, *544*, 271–297.
16. Sonnichsen, C.; Reinhard, B. M.; Liphardt, J.; Alivisatos, A. P. A Molecular Ruler Based on Plasmon Coupling of Single Gold and Silver Nanoparticles. *Nat. Biotechnol.* **2005**, *23*, 741–745.
17. Reinhard, B. M.; Sheikholeslami, S.; Mastroianni, A.; Alivisatos, A. P.; Liphardt, J. Use of Plasmon Coupling to Reveal the Dynamics of DNA Bending and Cleavage by Single EcoRV Restriction Enzymes. *Proc. Natl. Acad. Sci. U.S.A.* **2007**, *104*, 2667–2672.
18. Jun, Y. W.; Sheikholeslami, S.; Hostetter, D. R.; Tajon, C.; Craik, C. S.; Alivisatos, A. P. Continuous Imaging of Plasmon Rulers in Live Cells Reveals Early-Stage Caspase-3 Activation at the Single-Molecule Level. *Proc. Natl. Acad. Sci. U.S.A.* **2009**, *106*, 17735–17740.
19. Aaron, J.; Travis, K.; Harrison, N.; Sokolov, K. Dynamic Imaging of Molecular Assemblies in Live Cells Based on Nanoparticle Plasmon Resonance Coupling. *Nano Lett.* **2009**, *9*, 3612–3618.
20. Eustis, S.; El-Sayed, M. A. Why Gold Nanoparticles Are More Precious Than Pretty Gold: Noble Metal Surface Plasmon Resonance and Its Enhancement of the Radiative and Nonradiative Properties of Nanocrystals of Different Shapes. *Chem. Soc. Rev.* **2006**, *35*, 209–217.
21. Anker, J. N.; Hall, W. P.; Lyandres, O.; Shah, N. C.; Zhao, J.; Van Duyne, R. P. Biosensing with Plasmonic Nanosensors. *Nat. Mater.* **2008**, *7*, 442–453.
22. Reinhard, B. M.; Yassif, J. M.; Vach, P.; Liphardt, J. Plasmon Rulers as Dynamic Molecular Rulers in Enzymology. *Methods Enzymol.* **2010**, *475*, 175–198.
23. Loo, C.; Lowery, A.; Halas, N.; West, J.; Drezek, R. Immunotargeted Nanoshells for Integrated Cancer Imaging and Therapy. *Nano Lett.* **2005**, *5*, 709–711.
24. McStay, G. P.; Salvesen, G. S.; Green, D. R. Overlapping Cleavage Motif Selectivity of Caspases: Implications for Analysis of Apoptotic Pathways. *Cell Death Differ.* **2008**, *15*, 322–331.
25. Averitt, R. D.; Sarkar, D.; Halas, N. J. Plasmon Resonance Shifts of Au Coated Au_2S Nanoshells: Insight into Multicomponent Nanoparticle Growth. *Phys. Rev. Lett.* **1997**, *78*, 4217.
26. Zhou, H. S.; Honma, I. I.; Komiyama, H.; Haus, J. W. Controlled Synthesis and Quantum-Size Effect in Gold-coated Nanoparticles. *Phys. Rev. B: Condens. Matter Mater. Phys.* **1994**, *50*, 12052–12056.
27. Oldenburg, S. J.; Averitt, R. D.; Westcott, S. L.; Halas, N. J. Nanoengineering of Optical Resonances. *Chem. Phys. Lett.* **1998**, *288*, 243.
28. Stennicke, H. R.; Salvesen, G. S. Biochemical Characteristics of Caspases-3, -6, -7, and -8. *J. Biol. Chem.* **1997**, *272*, 25719–25723.
29. Kominami, K.; Nakabayashi, J.; Nagai, T.; Tsujimura, Y.; Chiba, K.; Kimura, H.; Miyawaki, A.; Sawasaki, T.; Yokota, H.; Manabe, N.; *et al.* The Molecular Mechanism of Apoptosis upon Caspase-8 Activation: Quantitative Experimental Validation of a Mathematical Model. *Biochim. Biophys. Acta* **2012**, *1823*, 1825–1840.
30. Shah, N. P.; Kasap, C.; Weier, C.; Balbas, M.; Nicoll, J. M.; Bleickardt, E.; Nicaise, C.; Sawyers, C. L. Transient Potent BCR-ABL Inhibition Is Sufficient to Commit Chronic Myeloid Leukemia Cells Irreversibly to Apoptosis. *Cancer Cell* **2008**, *14*, 485–493.
31. Asmussen, J.; Lasater, E. A.; Tajon, C.; Oses-Prieto, J.; Jun, Y. W.; Taylor, B. S.; Burlingame, A.; Craik, C. S.; Shah, N. P. MEK-dependent Negative Feedback Underlies BCR-ABL-mediated Oncogene Addiction. *Cancer Discovery* **2014**, *4*, 200–215.
32. Liu, L.; Xu, K.; Wang, H.; Tan, P. K.; Fan, W.; Venkatraman, S. S.; Li, L.; Yang, Y. Y. Self-assembled Cationic Peptide Nanoparticles as an Efficient Antimicrobial Agent. *Nat. Nanotechnol.* **2009**, *4*, 457–463.
33. Algar, W. R.; Malonoski, A.; Deschamps, J. R.; Blanco-Canosa, J. B.; Susumu, K.; Stewart, M. H.; Johnson, B. J.; Dawson, P. E.; Medintz, I. L. Proteolytic Activity at Quantum Dot-Conjugates: Kinetic Analysis Reveals Enhanced Enzyme Activity and Localized Interfacial "Hopping". *Nano Lett.* **2012**, *12*, 3793–3802.
34. Tassa, C.; Duffner, J. L.; Lewis, T. A.; Weissleder, R.; Schreiber, S. L.; Koehler, A. N.; Shaw, S. Y. Binding Affinity and Kinetic Analysis of Targeted Small Molecule-modified Nanoparticles. *Bioconjugate Chem.* **2010**, *21*, 14–19.
35. Wang, X.; Matei, E.; Deng, L.; Ramstrom, O.; Gronenborn, A. M.; Yan, M. Multivalent Glyconanoparticles with Enhanced Affinity to the Anti-Viral Lectin Cyanovirin-N. *Chem. Commun.* **2011**, *47*, 8620–8622.
36. You, C. C.; Agasti, S. S.; De, M.; Knapp, M. J.; Rotello, V. M. Modulation of the Catalytic Behavior of Alpha-Chymotrypsin

at Monolayer-protected Nanoparticle Surfaces. *J. Am. Chem. Soc.* **2006**, *128*, 14612–14618.
37. Prigodich, A. E.; Alhasan, A. H.; Mirkin, C. A. Selective Enhancement of Nucleases by Polyvalent DNA-functionalized Gold Nanoparticles. *J. Am. Chem. Soc.* **2011**, *133*, 2120–2123.
38. Jia, H.; Zhu, G.; Wang, P. Catalytic Behaviors of Enzymes Attached to Nanoparticles: The Effect of Particle Mobility. *Biotechnol. Bioeng.* **2003**, *84*, 406–414.
39. Mathis, R.; Hubert, P.; Dellacherie, E. Polyoxyalkyleneglycols Immobilized on Sepharose 6B for the Sequential Extraction of Three Enzymes From a Crude Extract of *Pseudomonas testosteroni*. *J. Chromatogr., A* **1989**, *474*, 396–399.
40. Ling, T. G. I.; Mattiasson, B. Poly(ethylene glycol)- and Poly(vinyl alcohol)-Substituted Carbohydrate Gels for "Mild" Hydrophobic Chromatography. *J. Chromatogr., A* **1983**, *254*, 83–89.
41. Gaertner, H. F.; Puigserver, A. J. Increased Activity and Stability of Poly(ethylene glycol)-Modified Trypsin. *Enzyme Microb. Technol.* **1992**, *14*, 150–155.
42. Lim, S. W.; Abate, A. R. Ultrahigh-Throughput Sorting of Microfluidic Drops with Flow Cytometry. *Lab Chip* **2013**, *13*, 4563–4572.
43. Ayala-Orozco, C.; Liu, J. G.; Knight, M. W.; Wang, Y.; Day, J. K.; Nordlander, P.; Halas, N. J. Fluorescence Enhancement of Molecules Inside a Gold Nanomatryoshka. *Nano Lett.* **2014**, *14*, 2926–2933.
44. Jang, J. T.; Nah, H.; Lee, J. H.; Moon, S. H.; Kim, M. G.; Cheon, J. Critical Enhancements of MRI Contrast and Hyperthermic Effects by Dopant-Controlled Magnetic Nanoparticles. *Angew. Chem.* **2009**, *48*, 1234–1238.
45. Yi, D. K.; Lee, S. S.; Papaefthymiou, G. C.; Ying, J. Y. Nanoparticle Architectures Templated by SiO2/Fe2O3 Nanocomposites. *Chem. Mater.* **2006**, *18*, 614–619.
46. Duff, D. G.; Baiker, A.; Edwards, P. P. A New Hydrosol of Gold Nanoclusters. *J. Chem. Soc., Chem. Commun.* **1993**, 96.
47. Duff, D. G.; Baiker, A.; Gameson, I.; Edwards, P. P. *Langmuir* **1993**, *9*, 2310.
48. Weiser, H. B. *The Colloidal Elements*; Wiley: New York, 1933.
49. Seo, D., Kim, J., Farlow, J., Lee, H., Cheon, J., Alivisatos, A. P., Gartner, Z. G., Jun, Y. Manuscript in preparation.
50. Zhang, X.; Servos, M. R.; Liu, J. Instantaneous and Quantitative Functionalization of Gold Nanoparticles with Thiolated DNA Using a pH-Assisted and Surfactant-Free Route. *J. Am. Chem. Soc.* **2012**, *134*, 7266–7269.
51. Joo, C.; Ha, T. Preparing Sample Chambers for Single-Molecule FRET. *Cold Spring Harbor Protoc.* **2012**, 1104–1108.
52. Edelstein, A.; Amodaj, N.; Hoover, K.; Vale, R.; Stuurman, N. Computer Control of Microscopes Using μManager. *Curr. Protoc. Mol. Biol.* **2010**, *92* 14.20 14.20.1−14.20.17.